Available online at www.sciencedirect.com

ScienceDirect

Proceedings of the Combustion Institute 38 (2021) 4757–4765

Proceedings of the Combustion Institute

www.elsevier.com/locate/proci

Thermal dynamics of deposited firebrands using phosphor thermometry

Yasin M. Abul-Huda*, Nicolas Bouvet

National Institute of Standards and Technology, 100 Bureau Dr. Gaithersburg, MD 20899, USA

Received 7 November 2019; accepted 14 July 2020
Available online 21 October 2020

Abstract

A series of experiments were carried out to identify and better understand the thermal mechanisms which govern the ignition propensity of firebrands. This work leverages the temperature-sensitive phosphorescence of YAG:Dy to non-intrusively measure and spatially resolve firebrand contact temperature along a 6.1 cm diameter area. The highly coupled firebrand heat transfer problem is studied by depositing smoldering firebrands onto a flat inert substrate and subjecting them to flow speeds of (1.5 $\pm$ 0.15) m/s. The temporal evolution of the thermal footprint is described and analyzed. Quasi-steady peak contact temperatures ranged between 500 K and 850 K while brief peaks exceeding 1150 K were also observed. The large difference in contact temperatures alludes to the significance in factors such as firebrand-fuel contact resistance, firebrand geometry, firebrand-flow orientation, fuel type (density and heat of combustion), and mass. Furthermore, the findings shed light on secondary heating events associated with shifting of the firebrand contact area and/or fragmenting, which can impart peak net heat flux equivalent to 70 % of the initial deposition. Lastly, considering the sensitivity of ignition on temperature, the work provides a brief discussion on the presence of unimodal and bimodal contact temperature distributions.
Published by Elsevier Inc. on behalf of The Combustion Institute.

Keywords: Firebrands; Temperature; Thermal footprint; WUI; Thermographic phosphors

1. Introduction

The generation, transport and deposition of firebrands, followed by ignition of recipient fuels, constitutes a chain of events rather common during Wildland–Urban Interface (WUI) fires [1]. Because of its severity, ignition by firebrands has received a fair amount of attention among the fire research community. Studies ranging from empirical approaches [2] to structural materials [3] to the development of analytical tools supported by semi-controlled laboratory-scale experiments [4] have been reported. Nevertheless, a comprehensive identification and understanding of the processes that govern firebrand ignition phenomena have proven elusive; complicated by the large number of variables and the complex coupling between them [5].

Recently, it was proposed to experimentally decouple fuel bed ignition from the firebrand, by investigating the thermal characteristics of firebrand piles alone [6,7]. The reported results were the first to provide a quantitative evaluation of the heat im-

* Corresponding author
E-mail address: yasin.abulhuda@gmail.com (Y.M. Abul-Huda).

https://doi.org/10.1016/j.proci.2020.07.098
1540-7489 Published by Elsevier Inc. on behalf of The Combustion Institute.

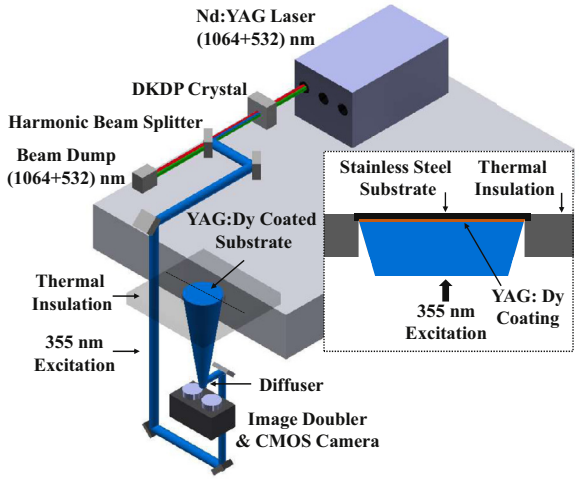

Fig. 1. Rendering of experimental setup. The insulation board makes up the bottom wall of a wind tunnel test section, which is omitted for clarity.

parted by firebrand piles. While doing so, it is important to acknowledge that the thermal contact resistance along the interface between a firebrand and a target fuel is likely to influence local heat transfer and therefore the ignition processes. Inhomogeneous and imperfect contact areas (firebrand surface irregularities associated with ash and char layers) may give rise to localized hot spots in the recipient fuel [8], that are difficult to capture with traditional measurement techniques. With the effect of spatially and temporally varying thermal conditions on recipient fuel ignitability being largely unknown, there is a need for performing measurements similar to those of refs [6,7], but at high spatial resolutions. Doing so may help formulate new ignition criteria for solid fuels based on the detailed thermal footprint of firebrands.

The present work is devoted to the measurement of two-dimensional thermal footprints of firebrands using a phosphor thermometry technique. The developed system allows for the time-resolved, high spatial resolution temperature mapping of an inert and thermally thin substrate, onto which are deposited glowing firebrands. The temporal evolution of the thermal footprint of firebrands located in a forced convective flow are investigated. The influence of factors such as the firebrand orientation with respect to the flow direction (parallel or perpendicular), firebrand quantity, firebrand geometry and mass are analyzed with respect to the evolution of the contact temperature mapping, and imparted energy to the substrate.

2. Experimental method and setup

For the sake of brevity, the following is only intended as a brief description of the experimental setup and approach. For more details, the reader may refer to the work of Abul-Huda [9].

2.1. Experimental setup

A rendering of the experimental setup is shown in Fig. 1. Ultraviolet light was produced with the third harmonic output of a pulsed Nd:YAG laser. The 355 nm beam was routed and expanded through a quartz glass diffuser to span the bottom surface of a 7 cm diameter stainless steel substrate. The bottom surface was coated with thermographic phosphors (see Section 2.2). The top surface of the substrate sat flush with a 50 mm thick ceramic fiber board that served to thermally insulate the sides. The substrate material (SS 304) and thickness (250 microns) were chosen for two reasons: (1) to minimize measurement intrusiveness by reducing the thermal mass (product of the density, specific heat, and volume); and (2) optimizing measurement accuracy by balancing the trade-off between minimizing lateral heat conduction and response time (approximately 10 ms), which are governed by the thermal conductivity and thermal diffusivity, respectively.

A CMOS camera (4096 × 3000, 12-bit) fitted with a f/2.8 lens and image doubler was positioned and focused to image the substrate-coated surface with an acquisition rate of 1 Hz. The in-house built image doubler permitted simultaneous acquisition of two images by effectively splitting the CCD sensor array in half. Each aperture was equipped with a series of optical filters to reject unwanted light and transmit light over two distinct spectral regions of emission [9]. The spatial resolution of the imaging system was approximately 40 μm. The ceramic fiber board that housed the substrate formed the bottom wall of a wind tunnel test section

Table 1
Virgin firebrand properties and specifications. The variables d, s, and th correspond to diameter, side, and thickness, respectively.

Geom.	Mat.	Dim. [cm]	Proj. Area [cm^2]	Mass [g]
Dowel	Maple	d:1 s:5	5.0	2.8
Square	Maple	th:1 s:2	4.0	3.3
Disc	Pine	d:5 th:0.6	18.8	7.4

(omitted from Fig. 1 for clarity). The blow-down type wind tunnel was comprised of a blower that pulled in ambient air through a series of honeycomb and screens to generate spatially uniform laminar flows with speeds of up to 8 m/s. In the present study, the freestream flow speed was fixed to (1.5 $\pm$0.15) m/s for all cases, and was directed parallel to the substrate surface. The speed lies in the middle of the range used by Ohlemiller [10] who investigated sustained smoldering propagation in wood. Visual observation of the deposited firebrand(s) was possible through a small viewing port in the top panel of the test section.

2.2. Thermographic phosphors

The use of thermographic phosphors for remote surface and gas thermometry has become an established technique [11,12]. YAG:Dy ($Y_3Al_5O_{12}$:Dy^{3+}) was the phosphor of choice because of its temperature sensitivity and range, emission intensity, resilience to phosphorescence degradation, and absorption and emission wavelengths. Temperature was inferred by the laser-induced phosphorescence intensity ratio of an image pair collected over two separate spectral regions centered around 458 nm and 500 nm. The expanded uncertainty in measuring temperature increased monotonically from $\pm$ 5.8 K to $\pm$ 45.6 K between 297 K and 1073 K, respectively [9]. The phosphors were adhered to the substrate using a mixture of distilled water and HPC binder (hydroxypropyl cellulose). The thickness of the cured phosphor coating was approximately 50 microns.

2.3. Firebrand preparation and deposition

The specifications of the three types of firebrands used in the present study are outlined in Table 1. The geometries are similar to those identified in previous firebrand studies [13,14] and can be easily replicated for future lab-scale studies. Details on what is known about the sizes and shapes of firebrands from actual fires can be found in Manzello et al. [1]. All firebrands were dried for 24 hours at 350 K prior to the experiments. Before being deposited onto the substrate, a firebrand was prepared by exposing it to a partially premixed propane flame for 20 seconds and was continuously moved around to form a uniform char layer. Next, it was removed from the propane flame and left in a self-sustained flaming state under a fume hood for 15 seconds. Lastly, the flame was blown out just before carefully depositing it onto the substrate in a glowing state. A pair of stainless steel pins (0.5 mm diam.) were used to nonintrusively prop (laterally) the firebrands and keep them from being convected away from the field-of-view. The pins present a negligible disturbance to the flow field (long and slender), have a contact area that is a fraction of a percent of the surface area of the firebrand, and masses that are a fraction of a percent of the substrate. Considering an energy balance, the heat losses through the pins are expected to be negligible and dominated by processes such as direct convective and radiative cooling of the firebrand.

3. Results

In the following sections, a time series capturing the contact temperature dynamics of each case is presented. The wind direction for all images is from top to bottom. For the first image in each series, dashed lines are used to denote diameters d = 2, 4, and 6 cm. Dash-dotted lines denote the approximate initial deposition location of the firebrand(s). Each case was repeated several times under nominally identical conditions to extract trends and conclusions that are believed to be independent of stochastic variations in the initial firebrand properties, preparation, deposition, and burning processes. Repeated trials for each case are provided in the supplemental material to provide a better understanding of the consistency/variability of the results.

This paper is organized by using the firebrand geometry as a convention to differentiate between cases. However, the reader is cautioned that differences in the trends discussed herein are not a sole manifestation of the firebrand geometry, but rather an artifact of a combination of factors including fuel geometry, flow-orientation, density, mass, heat of combustion, contact resistance, and effective surface contact area. Hence, attempts to perform direct comparisons between all cases should be refrained. Nevertheless, the results provide new insights into the thermal characteristics of firebrands, that to the authors' knowledge, have been widely unexplored.

3.1. Two-dimensional contact temperature mapping

For all cases, the smoldering fronts on the top surface of the firebrands moved from the edges towards the center. With the exception of the perpendicular dowel, the windward and leeward regions burned with the greatest intensity towards the center. For the perpendicular dowel, the most intense

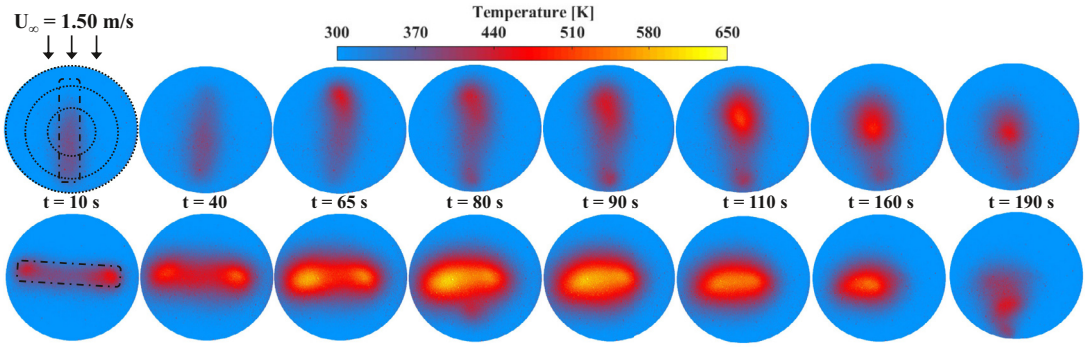

Fig. 2. Thermal footprint of dowel firebrands oriented parallel (top row) and perpendicular (bottom row) to the flow. Flow direction is from top to bottom. Dashed lines denote diameters of 2, 4, and 6 cm. (For interpretation of the references to color in this figure legend, the reader is referred to the web version of this article.)

burning occurred at the (left and right) ends and moved towards the center. These observations give a sense of where regions of heat release are greatest and where combustion-stabilizing flow interactions exist.

3.1.1. Significance of flow-fuel orientation

In this section, we explore the significance of the flow-fuel orientation on the heat transfer properties by orientating dowel-shaped firebrands either parallel or perpendicular to the flow. In the case of the parallel dowel, the leeward and windward ends was observed to glow intermittently. In the windward side, exothermic reactions released heat at a rate exceeding losses via convecting cooling. Overall, combustion was the most sporadic (between trials), mild in intensity, and inhomogenous compared to the other cases. On the other hand, the char oxidation dynamics were significantly more stable and intense in the perpendicular case. The smoldering front was observed to primarily move from the ends of the dowel toward the center. We speculate that the flow interaction with the blunt body forms a larger leeward recirculation region that entrains oxygen to stabilize combustion.

Figure 2 presents a time series of the thermal footprint of individual parallel (top) and perpendicular (bottom) dowel firebrands. The contact temperature of the parallel firebrands are generally lower and hover around 500 K. The mild nature of local exothermic reactions (in the form of smoldering) move between different regions as time elapses. The windward side of the dowel is the most intensely reacting region, but this is not always the case. A strong contrast is observed with the perpendicular dowel, where peak temperatures were observed to reach 650 K along the centerline of the dowel; a value approximately 30 % greater than the parallel configuration. The exothermic regions near the ends are sufficiently intense to help stabilize combustion along the length of the dowel ($10 \leq t$ (s) ≤ 80), releasing heat in a more spatially uniform manner. The greater burning intensity observed visually and alluded to by the measured contact temperatures is speculated to be caused by the larger momentum exchange between the firebrand frontal wetted area and incoming flow, which more effectively transports oxidizer through the firebrand char as compared to the diffusion process when the flow is oriented parallel to the surface of the firebrand. In addition, streaks of smoke were observed to be entrained into the leeward side of the firebrand, possibly serving as an additional mechanism for combustion stability. The larger drag forces break off parts of the firebrand that are observed to be entrained in the leeward recirculation region before being blown downstream ($t = 80$ s). The volume of the firebrand at $t = 110$ s is approximately half of when it was initially deposited. At $t = 190$ s, the firebrand is too small to be propped and is convected out of the field of view.

3.1.2. Significance of deposited firebrand quantity

Previous work has alluded to the significance of the physical characteristics of accumulated firebrands on the imparted heat flux [7]. It has been shown that heat of combustion and firebrand mass alone are not sufficient in determining net heat flux. Here we investigate the effect of deposited firebrand quantity on the thermal characteristics. No accumulation of ash was observed on the surfaces of individually deposited firebrands (all cases). However, this observation was drastically different in the case of two staged firebrands (where the second firebrand is positioned 4 mm downstream of the first), since the flow dynamics were sufficiently altered by the presence of the blunt and bluff bodies to form a stable insulating ash layer around both firebrands. This difference was inferred to be the cause of significant differences in the thermal characteristics.

The char layer oxidation was intense and stable for the square firebrands. The contact temperature maps of the single and dual square firebrands are

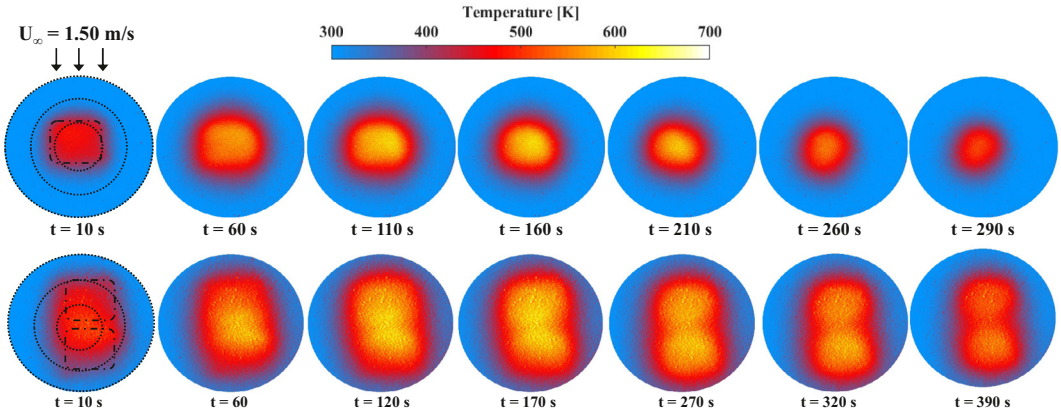

Fig. 3. Thermal footprint of single (top row) and dual-staged square firebrands (bottom row). Flow direction is from top to bottom. Dashed lines denote diameters of 2, 4, and 6 cm. (For interpretation of the references to color in this figure legend, the reader is referred to the web version of this article.)

shown in the top and bottom rows of Fig. 3, respectively. Upon initial deposition of a single firebrand, a uniform temperature of approximately 480 K is measured throughout the projected contact area. As time elapses, the core temperature increases and peaks to 600 K at 100 s. The thermal footprint becomes increasingly round, which is an artifact of lateral conduction through the substrate (smearing) and the drag forces that shear and round off the partially oxidized edges as the firebrand thermally degrades. The firebrand is continuously oxidized and fragmented, reducing the net heat transferred to the substrate and ultimately reducing the contact area and temperature.

In contrast, dual firebrands alter the flow dynamics to form an insulating ash layer that accumulates over both firebrands approximately 50 s after deposition. The ash layer was visually observed to shield the firebrands from the flow, reducing convective cooling and shearing of partially oxidized fuel, and sustaining burning times that were more than twice as long as the single firebrand case. From 60 s onward, the hottest regions were observed near the gap separating the firebrands, suggesting that a heat interaction between the two may exist. Small regions with peak temperatures of nearly 650 K were measured around 150 s, and sustained temperatures of 600 K remained until approximately 390 s.

3.1.3. Secondary heating events

The thermal footprint of a disc shaped firebrand is shown in Fig. 4. Immediately after deposition (t = 10 s), the largest temperatures are observed near the windward and leeward sides, corresponding with the glowing regions. While the square firebrand always sat flat against the substrate, the disc shaped firebrands took the form of hyperbolic paraboloids just before deposition and did not uniformly contact the substrate. This is believed to be due to a material stressing processes as the fuel thermally degraded, and may be associated with the grain direction and the relatively large surface area. In spite of this (t = 40 s), temperatures exceeding 550 K were measured throughout the projected area, and temperatures of approximately 600 K were measured at the windward and leeward regions. The relatively high temperatures in regions not in direct contact with the firebrand suggest that radiation may be a significant heat transfer mechanism.

At t = 50 s, the relatively large drag forces fracture the firebrand into two pieces. This is observed as the onset of a secondary heating event, causing temperatures in the center of the left fragment to briefly exceed 1150 K over a limited region (white). After fragmenting, the halves make better contact with the substrate since they more readily conform to the substrate surface. The gap between the halves registers elevated temperatures, suggesting that heat coupling between them may exist ($80 \leq t\ (s) \leq 140$). From this time onward, the temperatures of the fragments decay as they thermally degrade and partially oxidized fragments are swept downstream.

3.2. Trends in quantifiable data

3.2.1. Substrate stored energy

The stored energy per unit volume of the coated substrate was computed for each image in the time-series by integrating the energy contribution from each pixel *i*, through the following expression

$$E(t)=\frac{\sum_i \Delta T_i(t) A_p\left(\rho_{SS} C_{p_{SS}} \delta_{SS} + \rho_{YAG} C_{p_{YAG}} \delta_{YAG}\right)}{V} \quad (1)$$

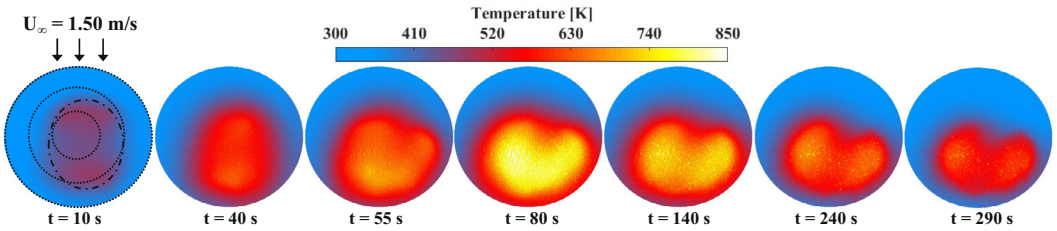

Fig. 4. Thermal footprint of a disc firebrand. Flow direction is from top to bottom. Dashed lines denote diameters of 2, 4, and 6 cm. (For interpretation of the references to color in this figure legend, the reader is referred to the web version of this article.)

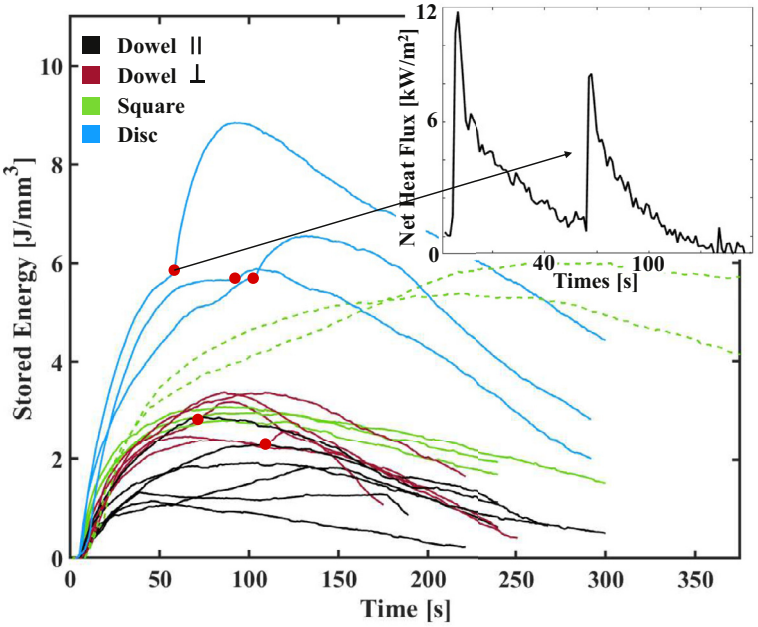

Fig. 5. Substrate stored energy per unit volume. Red circles denote the onset of secondary heating events. The inset is a segment of the net heat flux of a disc firebrand. (For interpretation of the references to color in this figure legend, the reader is referred to the web version of this article.)

where the subscripts *SS* and *YAG* denote stainless steel substrate and YAG:Dy coating, respectively. The variables t, ΔT, A_p, ρ, C_p, δ, and V represent time, temperature difference between the substrate and ambient, projected pixel area, density, specific heat, thickness dimension, and interrogated substrate and coating volume, respectively. As with any measurement technique, care should be taken in interpretation of this quantity since the thermal properties of the substrate affect the rate at which energy is transferred through and therefore from the substrate. From the results shown in Fig. 5, we first observe how the parallel dowels (black) impart less energy than the perpendicular orientation (red). Moreover, there is a significant spread between the energy profiles of different trials, owing to the relatively benign (flow-sensitive) and sporadic nature of combustion. In contrast, the perpendicular dowel case imparts larger and more rapid heat release to the substrate, and significantly less spread is observed between trials (more repeatable/stable combustion). Furthermore, the perpendicular firebrands burn and break apart faster (larger drag forces), leading to profiles that decrease more rapidly after they peak between 50 s and 100 s. The results show the importance of capturing the firebrand orientation, since the total imparted energy (area under each curve) can vary by a factor greater than two.

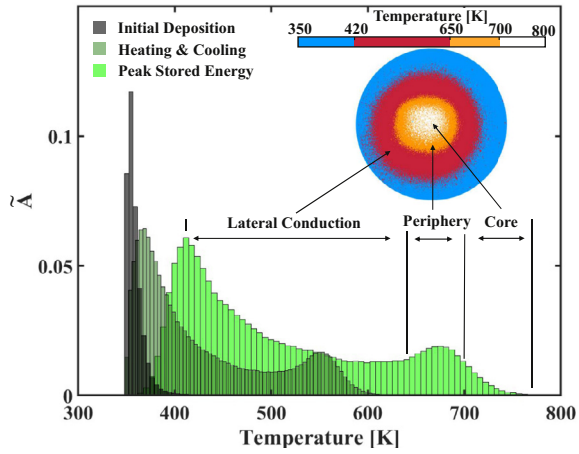

Fig. 6. Contact temperature PDF snapshots for a single disc firebrand at various times after deposition. $\tilde{A}$ is nondimensionalized area. The inset is a temperature-binned image that corresponds to a time of peak stored energy. (For interpretation of the references to color in this figure legend, the reader is referred to the web version of this article.)

The single square shaped firebrand cases (solid green) exhibit very stable and repeatable substrate-stored energy profiles. In addition, the profiles do not decay as rapidly as the perpendicular dowels. These observations are believed to result from the slightly larger mass and contact area of the firebrand which serves to insulate the underside of the firebrand from convective cooling (discussed in more detail below). The energy profiles of the dual square-shaped firebrands (dashed green) case are significantly different. Doubling the mass by staging a second firebrand more than doubles the imparted energy and the duration of energy transfer (burning time), as a consequence of the insulating ash layer that forms around both firebrands.

The disc shaped firebrands (solid blue) are observed to impart the largest energy to the substrate, as a consequence of factors including but not limited to, a larger mass and contact area. In some cases the firebrand shifts around, varying contact with the substrate. Moreover, it was susceptible to fragmenting into smaller pieces because of large drag forces. These two scenarios are termed secondary heating events and their onset is denoted by the red circles in Fig. 5. For example, the profile with the largest peak in Fig. 5 corresponds to the time series given in Fig. 4. The onset of the secondary heating event in this case is due to the firebrand fragmenting near t = 60 s. A second spike in net heat flux equivalent to 70 % of the initial deposition net heat flux was measured, as shown by the inset. The net heat flux is computed via the time rate of change of the spatially integrated stored thermal energy. The cause of the second peak is speculated to be a combination of: 1) improved firebrand-substrate contact associated with smaller (flatter) pieces; 2) increased thermal radiation originating from the new surfaces; and 3) brief increase in release of pyrolosates that subsequently oxidize and increase local temperatures. Secondary heating events were also prominent with perpendicular dowels and are therefore believed to be caused by large drag forces associated with larger firebrand frontal wetted areas.

3.2.2. *Contact temperature distributions*

The strength of the diagnostic is further leveraged to quantify the contact area temperatures by generating temperature probability density functions (PDFs) at various times after deposition. The PDFs can provide increased accuracy and detail to improve low order firebrand heating/ignition models which assume a single uniform (averaged) contact temperature. Figure 6 is an example of three temperature PDF snapshots of a disc firebrand taken soon after deposition (black), during a heating or cooling period (dark green), and around the time when the peak stored energy was observed (bright green). Heating and cooling periods are defined as times when the incident heat generated by the firebrand(s) is greater or less than the heat loss from the substrate, respectively. This can be seen visually in Fig. 5, where heating and cooling periods are associated with positive (soon after deposition) and negative slopes (later times) of the stored energy profiles, respectively. The y-axis is the integrated pixel area nondimensionalized by the projected area of the unburned firebrand.

With the exception of times immediately after initial deposition, the PDFs exhibit a bimodal distribution, and therefore can be broken down into three regions. The inset in Fig. 6 is given as an ex-

ample of a temperature-binned image corresponding to the three observed temperature regions of the 'Peak Stored Energy' PDF. The first region, referred to as the core (white), corresponds to a relatively small region with the highest temperatures. It is always observed near the center of a firebrand, and monotonically decreases in size with increasing temperature. Surrounding the core is a region referred to as the periphery (orange), which consists of an enclosed area of relatively lower temperatures. This region corresponds to the second peak in the bimodal distribution, and is approximately Gaussian in shape. For firebrands with larger contact areas (squares and discs), this region may serve to insulate the core from the flow, decreasing contact resistance and increasing heat transfer between the firebrand and the substrate. Lastly, a relatively large region is observed that is associated with areas dominated by lateral heat conduction through the substrate (red). This region decreases monotonically with increasing temperature. In the example shown, this region begins near 400 K, but can be different depending on the firebrand properties and time after deposition.

All of the cases under study exhibited similar qualitative trends in temperature distribution, with the exception of the parallel dowel and instances where firebrands fragmented into smaller pieces. The temperature PDFs of the parallel dowel were nearly monotonic in shape during all times after deposition, decreasing from a single peak near 350 K. Because there are limited areas of contact between the firebrand and surface, this orientation was not conducive to insulating the substrate surface directly underneath the firebrand from convective cooling. The temperature PDFs of the perpendicular dowel case transitioned between a bimodal and single peak distribution depending on the time after deposition.

It is important to note that the firebrand *contact* temperatures reported in this work are considerably lower than the firebrand *surface* temperatures published in Refs. [15,16]. Surface temperatures are reported in excess of 1200 K while the firebrand is suspended in a forced convection environment with negligible contact with another body/mass. This suggests that the thermal contact resistance associated with the irregularity of the firebrand surface and the substrate it is deposited over, and/or the accumulation of ash between them can significantly affect the local heat flux. Furthermore, the presence of a surface (or fuel bed) acts as a heat sink that reduces local temperatures on the firebrand surface, thereby decreasing local reaction rates and heat release.

4. Conclusions

The thermal dynamics of individual and dual firebrands was investigated using laser induced phosphorescence thermometry of YAG:Dy. The highly coupled firebrand heat transfer problem is studied by depositing smoldering firebrands onto an inert substrate. The findings show the significance of firebrand-flow orientation, contact area, contact resistance, the quantity of firebrands, and secondary heating events, on the thermal footprint and imparted energy.

Changing the firebrand flow configuration from parallel to perpendicular was shown to lead to a factor of two difference in the energy imparted to the underlying substrate. While parallel firebrands exhibited large variations in the imparted thermal energy between trials, the combustion of perpendicular firebrands were more stable and intense, leading to larger heat release rates and more repeatable (predictable) heat transfer to the substrate.

The heating dynamics of staging two firebrands was observed to be greater than the sum of its parts. Unlike with single firebrands, an ash layer accumulated over both firebrands, more than doubling the burning time and imparted energy to the substrate. This observation may also imply that radiation, as opposed to conduction and convection, may be a dominant mode of heat transfer in these scenarios, since considerable heat is still transferred through the ash layer to the substrate.

Secondary heating events, caused by firebrand shifting or fragmenting, were observed to impart peak net heat flux up to approximately 70 % of the initial deposition. This may have significant implications on fuel beds that have previously undergone a phase of preheating from initial deposition. These events were most prominent when large drag forces existed as in the cases with discs and perpendicular dowels.

The high spatial resolution provides more accurate measurements of the time-varying and spatially nonuniform thermal exposure of firebrands. The technique reveals how the periphery of the firebrand surface contacting the substrate surrounds a higher temperature core region, giving rise to a bimodal temperature distribution. Conventional methods leveraging thermocouples average local substrate temperatures, biasing values that may lead to inaccurate ignition criteria.

Declaration of Competing Interest

There are no competing interests to declare.

Acknowledgments

The authors acknowledge Stephen Fink, Ed Hnetkovsky, Cary Presser, Greg Linteris, Rodney Bryant, Jeffrey Eldridge, and Michael Gollner for technical support, loaning equipment, and helpful discussions.

Supplementary material

Supplementary material associated with this article can be found, in the online version, at doi:10.1016/j.proci.2020.07.098.

References

[1] S.L. Manzello, S. Suzuki, M.J. Gollner, A.C. Fernandez-Pello, *Prog. Energ. Combust.* 76 (2020) 100801.
[2] D.X. Viegas, M. Almeida, J. Raposo, R. Oliveira, C.X. Viegas, *Fire Technol.* 50 (2014) 61–77.
[3] S.L. Manzello, S.H. Park, T.G. Cleary, *Fire Safety J.* 44 (2009) 894–900.
[4] S.S. Wessies, M.K. Chang, K.C. Marr, O.A. Ezekoye, *Fire Technol.* 55 (2019) 1027–1056.
[5] A.C. Fernandez-Pello, *Fire Safety J.* 91 (2017) 2–10.
[6] R.S.P. Hakes, H. Salehizadeh, M.J. Weston-Dawkes, M.J. Gollner, *Fire Safety J.* 104 (2019) 34–42.
[7] J.C. Thomas, E.V. Mueller, R.M. Hadden, in: D.X. Viegas (Ed.), Coimbra, 2018, pp. 769–779.
[8] A. Warey, *Case Stud. Therm. Eng.* 12 (2018) 301–311.
[9] Y.M. Abul-Huda, *Development of a spatially resolved optical technique for measuring heat flux and thermal footprint of firebrand piles, NIST.TN.2052*, NIST, 2019.
[10] T.J. Ohlemiller, *Fire Safety Sci.* 3 (1991) 565–574.
[11] S. Allison, G. Gillies, *Rev. Sci. Instrum.* 68 (7) (1997) 2615–2650.
[12] M. Alden, A. Omrane, M. Richter, G. Sarner, *Prog. Energ. Combust.* 37 (2011) 422–461.
[13] S.L. Manzello, J.R. Shields, T.G. Cleary, A. Maranghides, W.E. Mell, J.C. Yang, Y. Hayashi, D. Nii, T. Kurita, *Fire Safety J.* 43 (2008) 258–268.
[14] J.P. Woycheese, in: Proceedings of the 9th Fire Science and Engineering Conference Proceedings (INTERFLAM), Interscience Communications, London, 2001, pp. 101–112.
[15] D.K. Kim, P.B. Sunderland, *Fire Safety J.* 106 (2019) 88–93.
[16] J.L. Urban, M. Vicariotto, D. Dunn-Rankin, A.C. Fernandez-Pello, *Fire Technol.* 55 (3) (2019) 1013–1026.